Earth's Future

RESEARCH ARTICLE
10.1029/2025EF007894

Artificial Flooding Leads to Thicker and Brighter Arctic Sea Ice

Edward Blanchard-Wrigglesworth[1], Andrea Ceccolini[2,3], Andrew Smith[2], Andrew Woods[2], Cían Sherwin[2], Konrad Borowski[2], Pascal Martin-Daguet[2], Simon Woods[2], Tom Clipston[2], Tommaso Di Gioacchino[2], Molly Wieringa[4], Jacob Pantling[5], Kate Oglethorpe[5], Shaun Fitzgerald[5], Steven Desch[6], Hilairy Hartnett[6,7], Brendan Kelly[8], Alison Tan[1], Bernard Steffin[9], Isaac Eskind[9], Brandon Langan[9], Brent Nakashook[10], Brian Kavanna[10], Brodie Larocque[9], David Kavanna[10], Roland Emingak[10], and Cecilia M. Bitz[1]

[1]Department of Atmospheric and Climate Science, University of Washington, Seattle, WA, USA, [2]Real Ice, London, UK, [3]Institute of Education – Psychology and Human Development, University College London, London, UK, [4]National Center for Atmospheric Research, Boulder, CO, USA, [5]Centre for Climate Repair, University of Cambridge, Cambridge, UK, [6]School of Earth and Space Exploration, Arizona State University, Tempe, AZ, USA, [7]School of Oceanography, University of Washington, Seattle, WA, USA, [8]International Arctic Research Center, University of Alaska Fairbanks, Fairbanks, AK, USA, [9]No Affiliations, [10]Ekaluktutiak Hunters & Trappers Organization, Cambridge Bay, NU, Canada

Key Points:

- We conducted a 2024/2025 fieldwork campaign to test the impact of flooding and melt pond draining on sea ice
- Sea ice flooded during the winter months was up to 32 cm thicker by early May and showed higher brightness, melting slower in spring
- Borehole drilling was effective in draining a melt pond within a week, leading to increased surface brightness within days

Supporting Information:

Supporting Information may be found in the online version of this article.

Correspondence to:

E. Blanchard-Wrigglesworth and A. Ceccolini,
edwardbw@uw.edu;
andrea@realice.eco

Citation:

Blanchard-Wrigglesworth, E., Ceccolini, A., Smith, A., Woods, A., Sherwin, C., Borowski, K., et al. (2026). Artificial flooding leads to thicker and brighter Arctic sea ice. *Earth's Future*, *14*, e2025EF007894. https://doi.org/10.1029/2025EF007894

Received 8 DEC 2025
Accepted 27 MAR 2026

Abstract We describe and present results from a 2024/2025 field campaign that is the first to test and observe the impact of flooding and meltwater draining on Arctic sea ice over the winter growth and spring melt seasons. The campaign was conducted in Cambridge Bay, Nunavut, Canada. A 1 by 1 km fieldwork site was used, comprising three control areas, which were never flooded, and eight test areas. In these, flooding treatments were carried out by pumping seawater onto the sea ice. Some test areas were flooded once (in December or January), while others were flooded twice (in December and February, or January and February). The total area flooded was 0.25 km^2. Additionally, one control area was used for a melt pond drainage experiment during spring. By mid May, prior to melt, flooded test areas were up to 32 cm thicker than control areas, with snow cover that was 1–13 cm thinner. Areas flooded twice exhibited greater thickening than those flooded once. During the melt period, sea ice in the flooded areas appeared brighter and showed slower melt rates, remaining thicker than that in the control areas. The drained melt pond site also brightened markedly within 1 week of borehole drilling. Comparison with a historical sea ice thickness record from Cambridge Bay indicates that a 30 cm increase corresponds to roughly the magnitude of long-term thinning observed over the past 50 years.

Plain Language Summary Arctic sea ice has been declining for the last few decades, and in the summer is expected to disappear by the middle of the century, causing further Arctic warming, coastal erosion, loss of wildlife, and impacting Arctic livelihoods. In response, several engineering approaches have been suggested to help slow down the loss of Arctic sea ice, such as stratospheric aerosol injection, surface albedo modification, or promoting sea ice thickening by flooding the surface with seawater during winter. This last idea has been tested in models, and here we document the first experiment to test it in the field with a small-scale (1 by 1 km) fieldwork campaign. Over the winter of 2024/2025, we flooded and monitored several test areas, while leaving control areas unaffected. We found that by the end of the winter sea ice growth season in mid-May, sea ice that had been flooded was up to 32 cm thicker than unflooded sea ice, equivalent to 50 years of thinning in the region. We also found that flooded sea ice was brighter during the melt season, leading to slower melt rates. In addition, a melt pond draining test in late May showed the surrounding area to effectively drain and brighten within days.

1. Introduction

Arctic sea ice has undergone significant decline in recent decades. Since 1979, annual Arctic sea ice extent has decreased by about 20%, September sea ice extent by about 40% (Cavalieri & Parkinson, 2012), and mean sea ice thickness has halved over the same period (e.g., Kwok, 2018). Most of the decline in sea ice loss over this period has been attributed to anthropogenic climate forcing (Gilbert et al., 2025; Kay et al., 2011; Notz & Stroeve, 2016; Roach & Blanchard-Wrigglesworth, 2022). Over much of the seasonal sea ice zone and along Arctic coastlines, the open-water season has lengthened by several weeks or even months (e.g., Rodrigues, 2009). These changes

© 2026. The Author(s).
This is an open access article under the terms of the Creative Commons Attribution License, which permits use, distribution and reproduction in any medium, provided the original work is properly cited.

have resulted in climatic impacts locally and afar, causing further Arctic warming (due to the sea ice albedo feedback, Stuecker et al. (2018)), and ecological and human impacts. The loss of sea ice and increased open water season has caused increased coastal erosion (Overeem et al., 2011), altered transport and hunting for Arctic communities (Dammann et al., 2018; Eicken & Mahoney, 2015; Hauser et al., 2021; Laidler et al., 2009), and increased energetic costs and mortality of sea ice-associated species such as polar bears, walruses, and seals (Archer et al., 2025; Kelly, 2001; Laidre et al., 2008; Molnár et al., 2020; Regehr et al., 2007).

While the magnitude of future sea ice loss is contingent on future emission scenarios, Arctic sea ice is expected to continue to decline over the next few decades, regardless of near-future emission pathways. End-of-summer sea ice is expected to be completely lost with global warming of 2°C over 2000 levels (Mahlstein & Knutti, 2012) and predicted to take place by the middle of the century, especially under future high or medium emissions scenarios (e.g., Jahn et al., 2024).

In light of past and expected future sea ice loss, several engineering approaches have been proposed to slow the rate of Arctic warming and sea ice loss. Modeling studies have explored stratospheric aerosol injection (e.g., Lee et al., 2023; Tilmes et al., 2014), increasing the Arctic's albedo by enhancing ocean albedo (Cvijanovic et al., 2015; Mengis et al., 2016), or increasing sea-ice albedo by adding reflective, hollow glass microbeads to the sea ice surface (Field et al., 2018). However, none of the proposed methods for modifying Arctic surface albedo have reversed the simulated negative trend in Arctic sea ice extent, and deploying glass microbeads may even accelerate the loss of Arctic sea ice loss (Webster & Warren, 2022).

An alternative proposal consists of flooding the surface of Arctic sea ice with seawater during the winter months (Desch et al., 2017). This idea has been tested with a variety of modeling methods (Desch et al., 2017; Pauling & Bitz, 2021; Zampieri & Goessling, 2019), in general finding that flooding the surface during winter leads to thicker sea ice the following spring, potentially slowing down the loss of Arctic sea ice by several decades. Pauling and Bitz (2021) pointed out that surface flooding in winter ultimately converts snow to snow-ice, which then raises heat conduction out of the ocean and results in basal sea ice growth that is several fold greater than the enhanced snow-ice production. These modeling studies warn that flooding snow too late in winter could be counterproductive, as they speculated that it would cause the sea ice to melt earlier.

To our knowledge, while recent efforts have been carried out to test the feasibility of sea ice surface flooding, no field campaign has attempted a full winter-to-melt season assessment of the impact of flooding on sea ice. Real Ice, a UK-based not-for-profit organization, first tested the seawater-on-sea ice pumping engineering in Nome, Alaska in March 2023, and in Cambridge Bay (Iqaluktuuttiaq), Canada in spring 2024, while similar tests have been carried out in Svalbard in spring 2024 by the Dutch company Arctic Reflections (Hammer et al., 2024). In this paper, we document a 2024/2025 field campaign led by Real Ice, which is the first to test and observe the impact of flooding and meltwater draining on Arctic sea ice over both the winter growth and spring melt seasons.

2. Data and Methods

The field campaign took place in Cambridge Bay, a small (approximately 8 × 3 km) bay along the south coast of Victoria Island in the Canadian Arctic Archipelago (see Figure 1), located at 69.1°N, 105°W. At the northwest head of the bay sits the town of Cambridge Bay. We chose Cambridge Bay for our fieldwork because it offered a sheltered bay with a long sea ice season (typically consisting of stable fast sea ice), consistently cold winters, and logistical support from the Canadian High Arctic Research Station and local Cambridge Bay Ekaluktutiak Hunters and Trappers Organization (EHTO) guides. The field work took place in a 1 × 1 km area at the eastern end of the bay, about 7 km southeast from the town of Cambridge Bay. Within the 1 × 1 km work area, 11 different sites of 100 m radius were selected as either control areas (three sites) or test areas (eight sites, see Figure 2a). Within the control areas, no flooding was performed at any time. Within the test areas, flooding was performed during one or two different time windows throughout the winter. Three different flooding periods were performed; a late November–December period (27 November–12 December, hereafter "Flood-Dec"), a mid-late January period (15 January–31 January, hereafter "Flood-Jan"), and a mid February period (12 February–21 February, hereafter "Flood-Feb"). To test the impact of flooding timing and frequency on sea ice thickness, different test areas were flooded alternatively during these periods, either just once or twice in total. Test areas R1 and R2 were flooded only once in December, R3 and R4 were flooded twice in December and February ("Flood-DF"), R5 and R8 were flooded once in January, and R6 and R7 were twice in January and February ("Flood-JF").

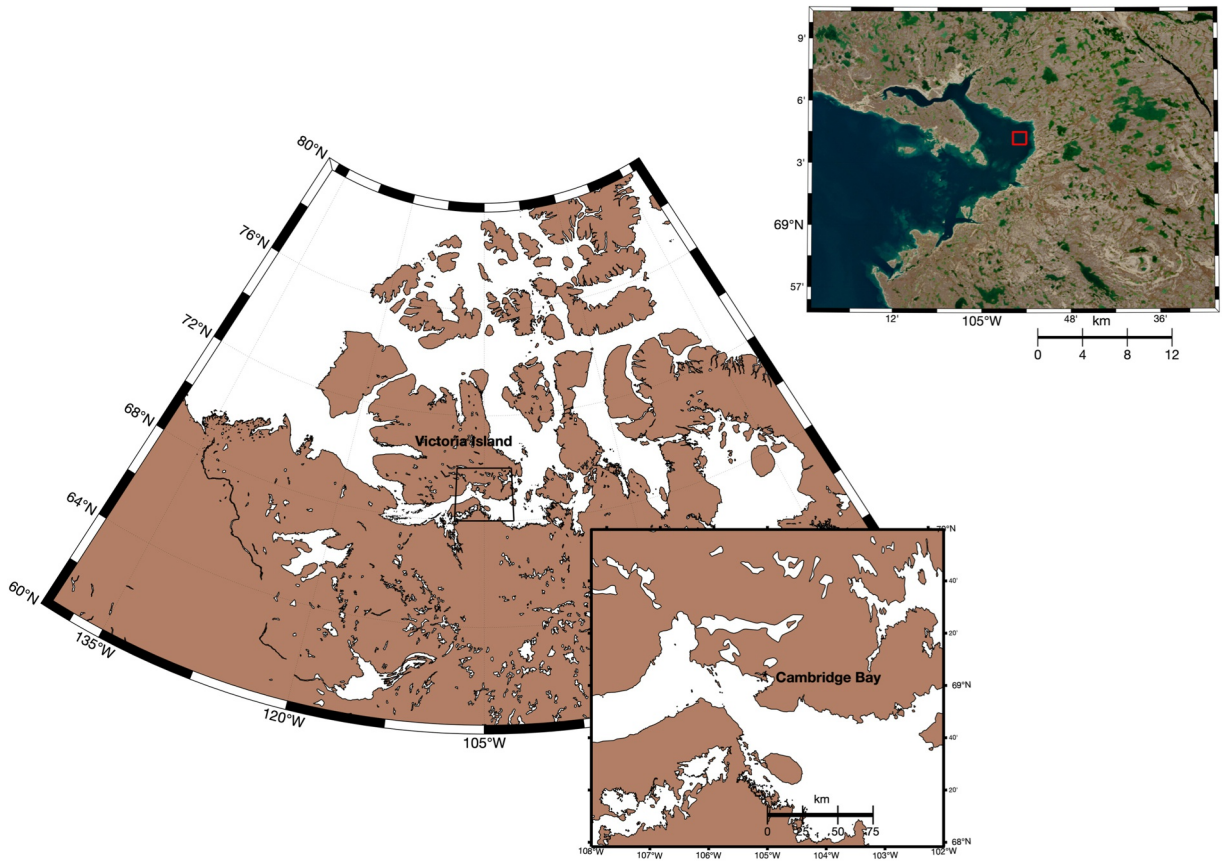


Figure 1. Location of Cambridge Bay. The red box indicates the campaign site.

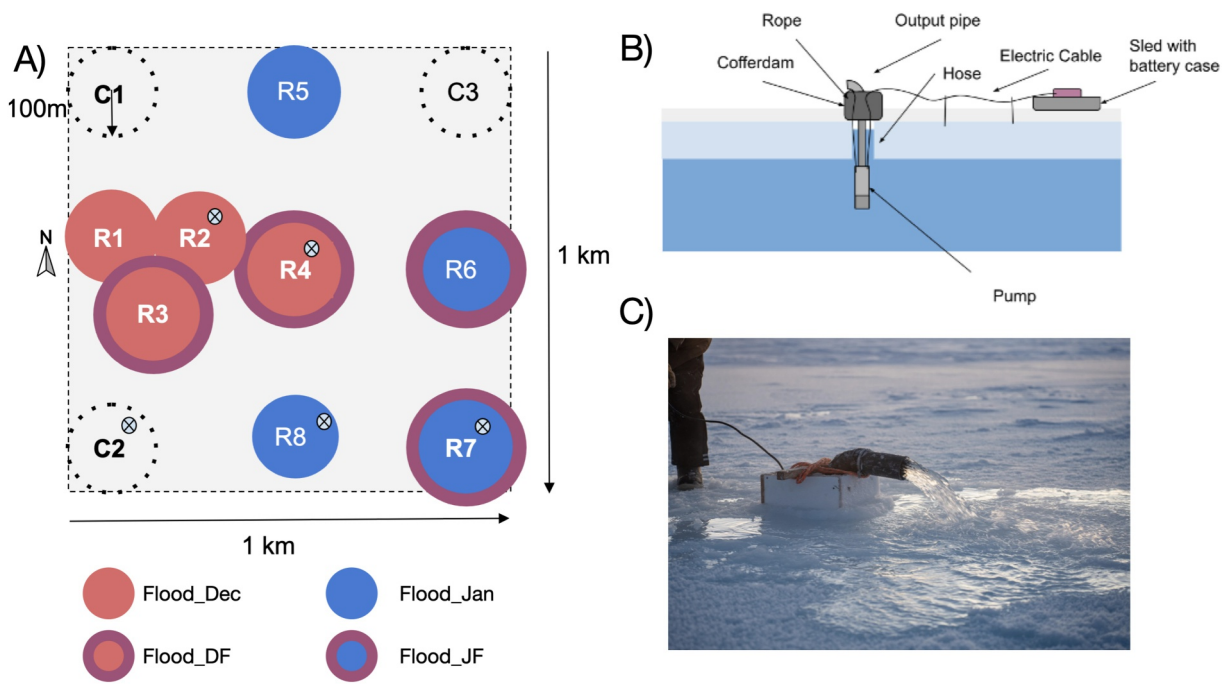


Figure 2. (a) Design of the test site in Cambridge Bay, (b) Schematic of the pumping system. The vertical scale is approximately 2–3 m; the pump outlet sits approximately 50 cm above the surface. (c) pumping sea water onto the ice.

Table 1
Summary of Campaign

Observation dates	Flooding/drill dates	Mean date of obs. Samples	Areas flooded/melt pond drain	# Ice thickness obs.	# Snow depth obs.
26 November−14 December	27 November−12 December	4 December (C), 5 December (R)	R1, R2, R3, R4	191	117
14 January–31 January	15 January–31 January	21 January (C), 24 January (R1, R4), 22 January (R5, R8)	R5, R6, R7, R8	113	110
12 February–23 February	12 February–21 February	19 February (C), 19 February, (R1, R2), 18 February (R5, R8), 20 February, (R3, R4), 20 February (R6, R7)	R3, R4, R6, R7	306	302
March 15–April 20	N/A	6 April (C), 10 April (R1, R2), 6 April (R5, R8), 6 April (R3, R4), 6 April (R6, R7)	N/A	161	161
May 3–May 15	May 29	11 May (C), 10 May (R1, R2), 11 May (R5, R8), 9 May (R3, R4), 11 May (R6, R7)	Melt pond drain (C2)	228	228

Note. Observation dates lists the dates over which ice thickness, snow depth, or ice core observations were taken, Flooding/drill dates described the dates when flooding or melt pond drilling were performed. C and R refer to all control or test areas respectively.

The flooding set up consisted of a pump–pipe connected to an electric battery. The pump–pipes were placed in a drilled borehole, with the pump inlet about 2 m below the surface, and the outlet about 0.5 m above the surface, supported by a wooden cofferdam, which also stopped pumped water on the sea ice surface from flowing back into the borehole before refreezing (Figures 2b and 2c and Movie S1). Each individual pumping cycle would last approximately 3:45 hr and pump 48 m^3 hr^{-1}. A total of four pumps were used. After each individual pumping cycle, the pump would be relocated to another location within the vicinity for another cycle. For the whole campaign, the total volume of water pumped was around 30,000 m^3, flooding an area of 0.25 km^2. At the end of each pumping cycle, the perimeter of the flooded area was mapped with GPS and the pump was relocated within the same test area so a new pumping cycle could be performed. The snow on sea ice was not removed prior to pumping. In most cases, we observed the pumped water would saturate the pre-existing snow layer and spread horizontally. The saturated snow layer would then quickly freeze into snow-ice, with no snow left over the following few hours.

We also explored the effects of intentional melt pond drainage in one of the control areas (C2). This was done during the melt season on 29 May by drilling a dozen 5 cm boreholes through the ponded sea ice, within about a 50 m radius of the central C2 area marker. This area was subsequently monitored daily via drone. Table 1 summarizes the individual flooding and observing periods.

Throughout the winter and spring, measurements of sea ice thickness, snow depth, and bulk sea-ice salinity profiles were taken in all control and test areas. A total of 1,040 sea ice thickness measurements, 923 snow depth measurements, and 59 sea ice bulk salinity profiles were taken. Sea ice thickness was measured by drilling boreholes through the sea ice and using a Kovacs ice thickness gauge. Snow depth was measured with a snow probe. Both measurements have an accuracy of 1 cm, which is much smaller than the small scale variability in both metrics. We assess statistical significance of the differences between test and control areas with the Wilcoxon rank sum test and the two-sample Kolmogorov-Smirnov test. The salinity profiles were measured from extracted ice cores (see the Supporting Information S1 for details on salinity measurements and calibration). Each ice core was sampled in 10 cm long sections, from top to bottom.

We also installed four Snow and Ice Mass Balance Arrays (SIMBAs, Jackson et al., 2013). SIMBAs measure the environmental temperature at 2 cm intervals along a 5 m long thermistor string. Two SIMBAs, installed in R4 and R7, recorded continuously from January through July. One SIMBA, installed in C2, recorded from January until February when it was damaged by wildlife. A fourth SIMBA was installed in R3 in January and operated until 10 April, after which it was relocated to C1 on 14 May. The SIMBA strings were installed in a borehole, supported by a tripod placed on top of the sea ice. In addition to monitoring ambient air, sea ice, and ocean temperature, the temperature profiles can also be used to derive sea ice thickness and snow depth by identifying air/snow/sea ice/ocean interfaces using the temperature gradient contrasts at the interfaces with a precision of 2 cm (Plante et al., 2024). During the melt season, when temperature gradients are too small to identify the interfaces, we use estimates of the temperature boundary conditions to locate the top and bottom of the sea ice. For the top (air/sea ice) interface, we use the freshwater melting point of 0°C, which assumes a rapid desalination of the top sea ice

layer (e.g., Holt & Digby, 1985; Malmgren & i Bergen. Geofysisk institutt, 1927). The temperature at the sea ice/ocean interface depends on the seawater salinity, which we did not measure, so we use a range of temperature spanning −0.2 to −1.5°C. We calculate the lower threshold using ocean salinity measurements from Ocean Networks Canada taken offshore Cambridge Bay.

During spring, airborne drone surveys were conducted to monitor surface changes across the entire 1 × 1 km study area. We derived surface luminance from daily drone orthomosaic composites to track relative brightness differences between test and control areas throughout the melt season. While luminance data are not albedo measurements, they provide a useful proxy for relative surface brightness by comparing luminance ratios between test and control areas. Drone images were acquired using a DJI FC9113 RGB camera. These images are automatically gamma-encoded when stored, a non-linear transfer function commonly used to match images to the perceptual sensitivity of the human visual system (Nguyen & Brown, 2017). For quantitative comparison of surface brightness across test and control areas, this nonlinearity must be removed through a process of linearization, so that pixel values are proportional to scene radiance. Details of the luminance derivation from in-camera RGB recordings are provided in the Supporting Information S1.

Satellite observations from ESA-Sentinel (Sentinel-2 L2A) were also used during the spring melt season to monitor changes. This data set provides visible high-resolution imagery at 5 m per pixel resolution during the polar day.

We use ERA5 (Hersbach et al., 2020) and Cambridge Bay airport 2-m surface air temperature to characterize historic and 2024/2025 winter conditions, and to contextualize any impacts from the sea ice flooding. We also use weekly sea ice thickness measurements taken offshore in the town of Cambridge Bay by Environment Canada and available annually since 1960 (Howell et al., 2016). While these are in a different location in the bay from the field site, the sea ice thickness measurements provide valuable insight into historic trends and help frame the campaign's results.

3. Results

We begin by characterizing historic and winter 2024/2025 conditions in Cambridge Bay. Mean winter (December through April, DJFMA) temperatures have significantly warmed since the 1970s, with 1980–2025 DJFMA warming rates of 0.58°C per decade at Cambridge Bay airport (0.54°C per decade using ERA5 data, Figure 3a). At the same time, maximum annual sea ice thickness at Cambridge Bay has declined, from values centered around 220 cm in the 1960s and early 1970s to 200 cm or lower in recent decades, reflecting a 1980–2024 trend of −6 cm per decade (Figure 3b). As documented by Howell et al. (2016), annual sea ice maxima are partly driven by winter temperatures (correlation $r = -0.62$), with warmer winters leading to thinner sea ice maxima (Figure 3c).

During autumn 2024, surface air temperature first significantly dropped below freezing during the last week of October, with daily mean temperatures dropping to −10°C by 1 November (Figure 3d). The bay started to freeze in the last week of October 2024, and was fully covered in sea ice by Nov 1, as estimated using both remote sensing (NASA Worldview and MASIE sea ice concentration products) and in situ reports from local observers. This was a relatively late date of sea ice freeze up for the region, consistent with later sea ice freeze-up in recent decades (e.g., Lebrun et al., 2019). Surface air temperature remained below freezing until May 22, after which daily mean temperatures remained above freezing for the rest of the melt season. The winter of 2024/2025 was anomalously warm in Cambridge Bay, the third warmest on record at 4°C above the 1981–2010 climatology (Figure 3), and 2.5°C above the 1970–2024 linear trend projected to 2025. Given the long term trend of 0.58°C per decade, and assuming a continuation of the observed trend, the winter of 2024/2025 can be expected to become a typical winter by 2070.

3.1. Flooding Impacts During the Sea Ice Growth Season

To illustrate the impact of flooding during the sea ice growth season, we first show the time-evolution of sea ice thickness and snow depth, using both the direct observations and the SIMBA estimates (Figure 4), as well as the full end-of-winter sea ice thickness and snow-depth measurements (Figure 5). Sea ice thickness and snow depth values are summarized in Table 2 and Table S1 in Supporting Information S1.

For each observing period, the mean date on which observations were taken at each site can differ by 1–3 days, and observations prior to flooding tend to lead those over test areas after flooding (see Table 1). Since mean sea

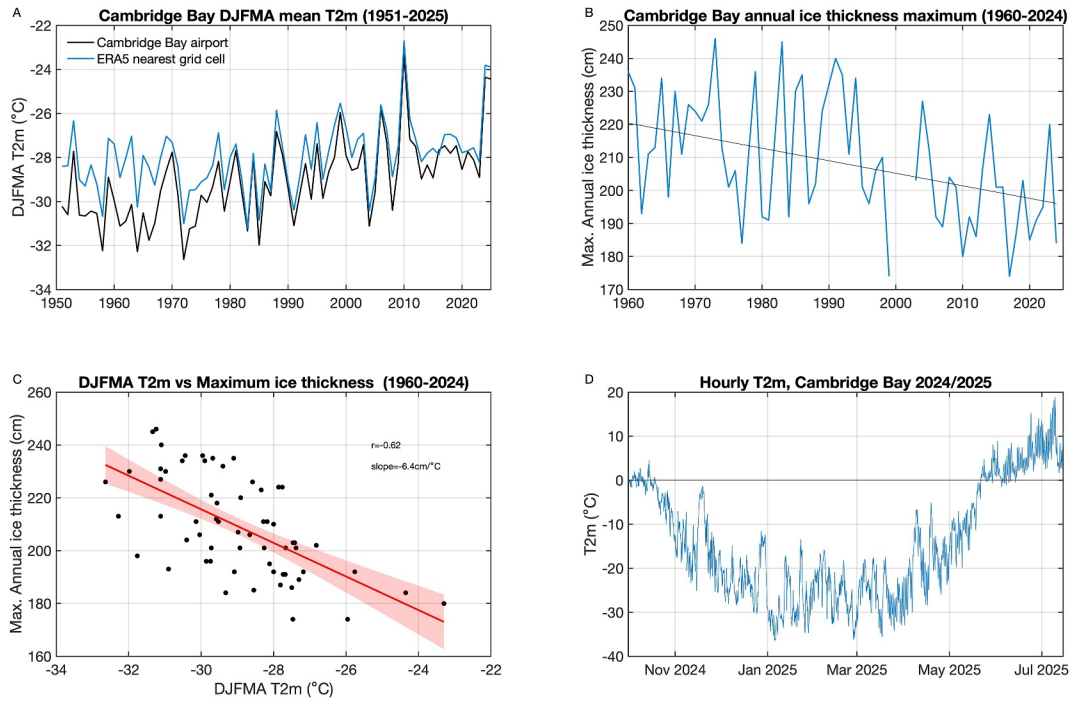


Figure 3. (a) Mean winter (December through April) temperature at Cambridge Bay, using the Cambridge Bay airport observations (black), and as estimated by ERA5 (blue), 1951–2025, (b) Maximum sea ice thickness at Cambridge Bay for 1960–2024, using data from Environment Canada, with the best-fit linear trend shown in black, (c) scatter plot of winter temperature and maximum annual ice thickness, 1960–2024. The red fit shows the linear regression, with a 90% confidence interval (d) hourly surface temperature at Cambridge Bay airport, October 2024–July 2025.

ice growth rates are ∼1 cm per day, to compare control and test areas over a fixed date range, we have calculated best-fit models of all sea ice thickness observations. We found that a polynomial of order 2 model provided the best fit. We calculate model mean values over periods lagged a few days from the flooding windows (1–11 December, 16–26 January, 16–26 February, 3–15 May, Figure 4a and Table 2). For snow depth measurements, which are more variable in time and space and for which a best-fit model is not as appropriate as for sea ice thickness, we show the mean and medians of all observations taken throughout the campaign (Figure 4b and Table 2). For completeness, we also show the equivalent mean and median sea ice thickness in Table S1 and Figure S3 in Supporting Information S1.

For the unflooded sea ice observations (control test areas and observations in the test areas prior to any flooding), mean ice thickness evolved from 53 cm thick during 1–11 December, 98 cm thick during 16–26 January, 122 cm thick during 16–26 February, to 161 cm during 3–15 May, the end of the ice growth season (Figure 4a). For the test areas only flooded in December, mean ice thickness evolved from 65 cm thick during 1–11 December, 109 cm thick during 16–26 January, 133 cm thick during 16–26 February, to 174 cm during 3–15 May. For the test areas only flooded in January, mean ice thickness evolved from 114 cm thick during 16–26 January, 141 cm thick during 16–26 February, to 181 cm during 3–15 May. For the test areas flooded twice in December and February, mean ice thickness evolved from 147 cm thick during 16–26 February, to 190 cm during 3–15 May. For the test areas flooded twice in January and February, mean ice thickness evolved from 147 cm thick during 16–26 February, to 192 cm during 3–15 May. The SIMBA ice thickness tendency estimates, which are available near-continuously in time, show good agreement with the direct observations and the best-fit models (Figure 4a).

To further assess the impact of flooding on end-of-winter sea ice thickness, we compare ice thickness across the control and test areas between May 3 and May 15 (Figure 5a). Median ice thickness in the control areas was 162 cm, with an inter-quartile range (IQR) of 153–172 cm. In the December-only flood areas, ice thickness was 175 cm (IQR 169–180 cm); in the January-only flood areas, ice thickness was 184 cm (IQR 178–187 cm). The thickest sea ice was found in the test areas that had been flooded twice; in the December and February flood areas, ice thickness was 190 cm (IQR 185–197 cm), while in the January and February flood areas, ice thickness was

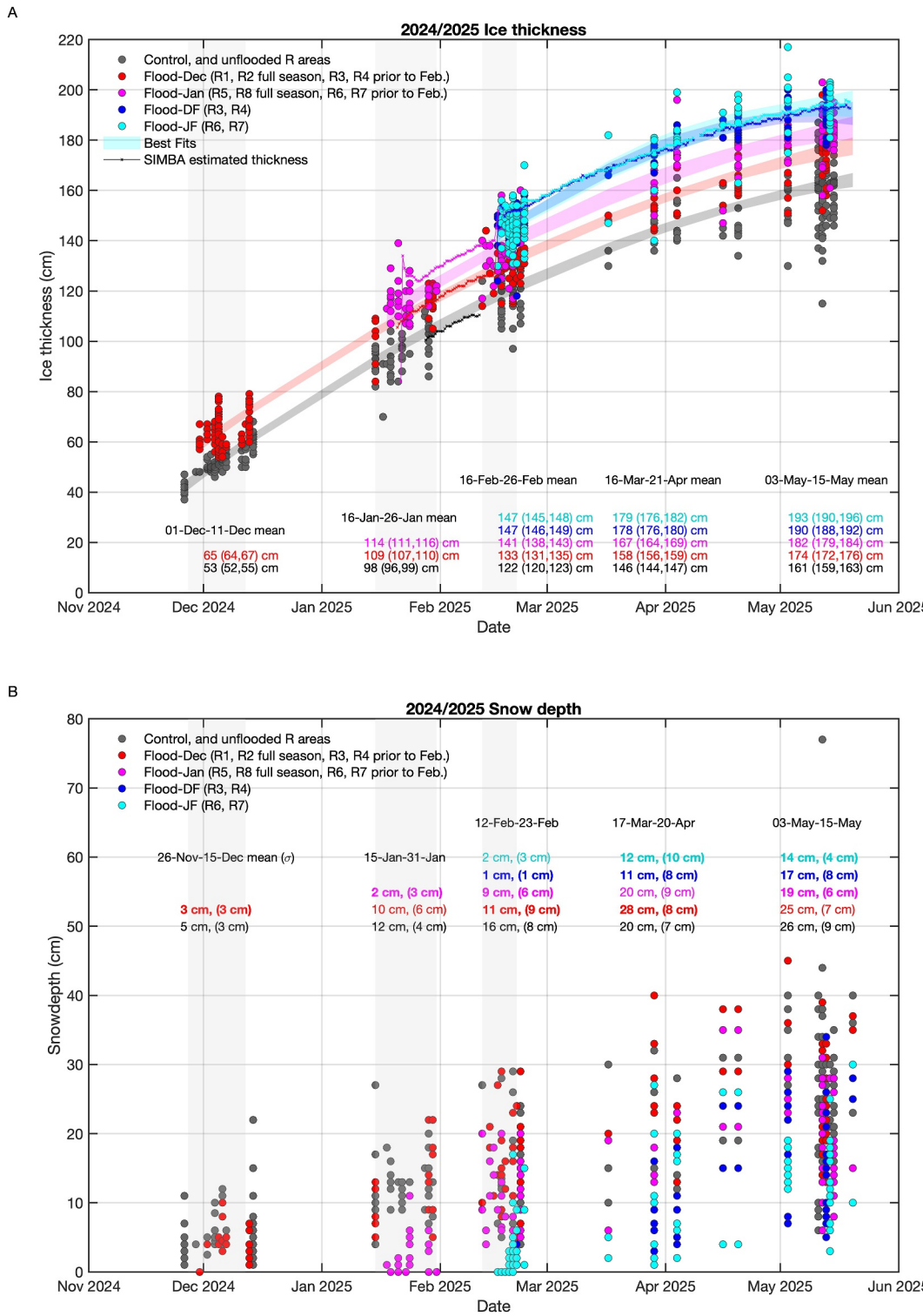


Figure 4. (a) Sea ice thickness measurements, with models of best-fit, showing the 90% confidence intervals. Control and pior-to-flooding test areas are shown in black, December-only flooded in red, January-only flooded in magenta, December and February flooded in blue, and January and February flooded in cyan. Labeled values show the mean ice-thickness from the best-fit model during the different date ranges displayed. Panel (b) as in panel (a), but for snow depth. The labeled measurements provide the mean (standard deviation) values during the different time windows. Bold labels indicate statistically significant differences with respect to the control. Flooding windows highlighted in gray shading.

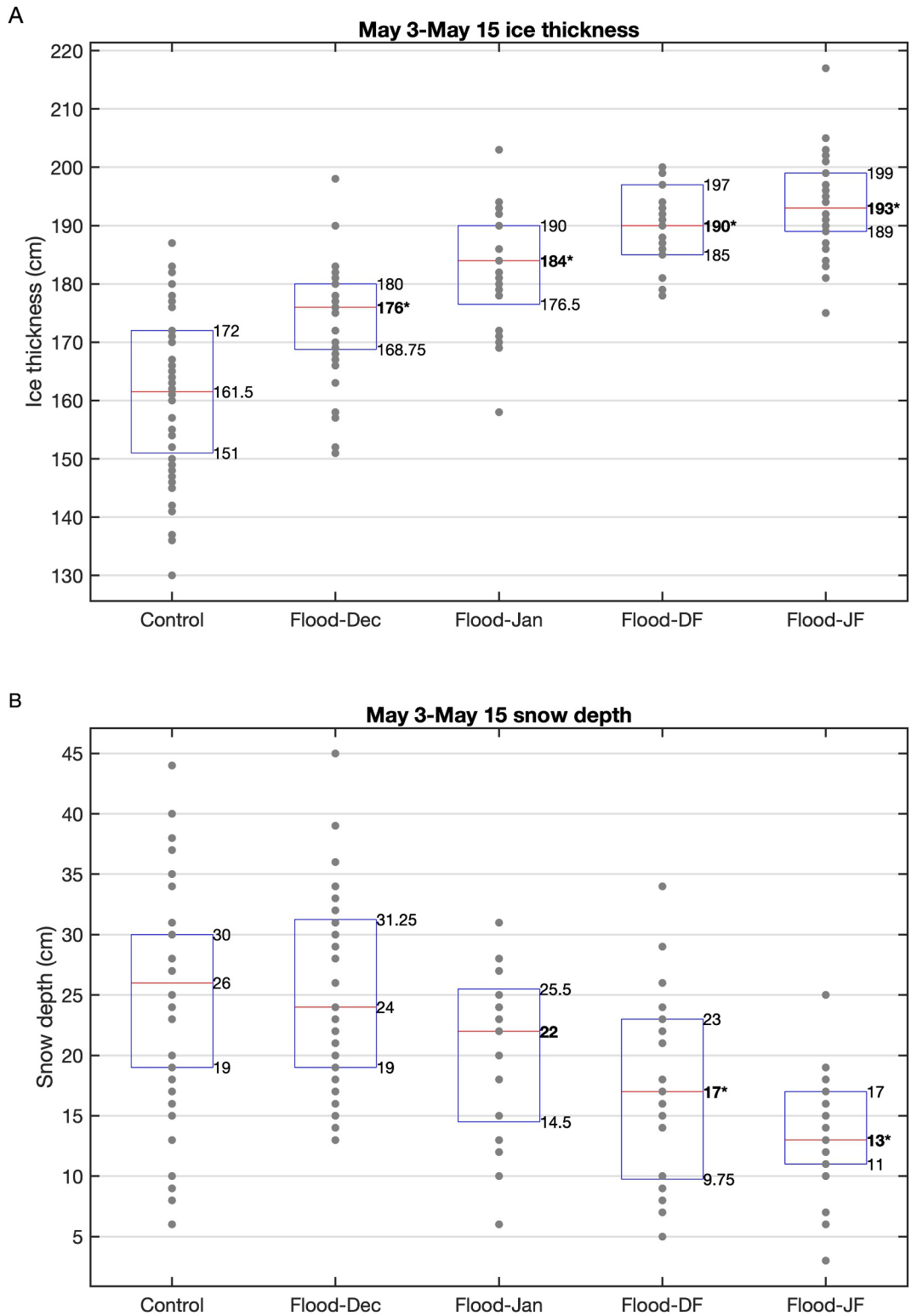


Figure 5. (a) May 3–May 15 sea ice thickness at the control areas (left column), single flooded in December (R1, R2) or January (R5, R8) test areas, those flooded both in December and late February (R3, R4), and those flooded both in January and February (R6, R7). The boxplot show the 25, 50, and 75th percentiles, gray dots show all data. Panel (b) as in panel (a), but for snow depth. Test area median values are highlighted in bold when 95% significantly different to control median values, and have an asterisk when 99% significantly different to control median values.

Table 2
Ice Thickness and Snow Depth

Ice thickness (cm), best-fit values, mean (90% confidence intervals)						
Areas	December 1–10	January 16–26	February 12–21	March 15–April 20	May 3–15	Diff. from Control, in May, *or post-flooding in italics*
Control & unflooded test	53 (52,55)	97 (96,99)	121 (120,123)	146 (144,147)	161 (159,163)	
Flood-December (R1, R2, R3, R4)	65 (64,67)	109 (107,110)	133 (131,135)	158 (156,159)	174	13, *12*
Flood-January (R5, R6, R7, R8)		114 (111,116)	141 (138,143)	167 (164,169)	182 (179,184)	21, *17*
Flood-DF (R3, R4)			147 (146,149)	178 (176,182)	190 (188,192)	29, *26*
Flood-JF (R6, R7)			147 (145,148)	179 (176,182)	193 (190,196)	32, *26*
Snow depth (cm), mean, *median in italics*, (number of obs in parenthesis)						
Areas	December	January	February	March–April	May	Diff. from Control, in May
Control & unflooded test	5,*4* (78)	12,*10* (44)	16,*14* (43)	20,*20* (42)	26,*25* (93)	
Flood-December (R1, R2, R3, R4)	**3,*4*** (39)	10,*10* (17)	**11*,*12*** (59)	**28*,*29*** (13)	25,*23* (40)	−1, −*2*
Flood-January (R5, R6, R7, R8)		**2*,*0*** (49)	**9*,*8*** (45)	20,*20* (28)	**19*,*18*** (38)	**−7*, −*7***
Flood-DF (R3, R4)			**1*,*1*** (62)	**11*,*9*** (28)	**17*,*17*** (25)	**−9, −*9***
Flood-JF (R6, R7)			**2*,*1*** (93)	**12*,*9*** (28)	**14*,*13*** (32)	**−12*, −*13***

Note. For ice thickness values, we show the mean values from the best-fit models (see Figure 4) for December 1–10, January 16–26, February 12–21, and May 3–15. The difference from control sea ice thickness values show the difference during May 3–15, and in parenthesis, the difference immediately following the flooding window. For snow values, we show the mean and median (in italics) values for each observing period, using all observations. Flood snow depth values are boldened/have asterisk when 95% or 99% statistically significantly different to control/pre-flooded values. For ice-thickness, all flood best-fit models are 99% statistically significant from the control/pre-flooded best-fit model.

193 cm (IQR 189–199 cm). Thus, sea ice was on average 13 cm thicker if flooded in December, 22 cm thicker if flooded in January, and 28–31 cm thicker if flooded twice—all values are statistically significant (see Table S2 in Supporting Information S1). To explore the time evolution of the difference between the flooded and the unflooded areas, we assess the difference in thickness immediately following the flooding windows of each test area, and the difference by end of the season (see Table 2 and Figure 4a). Most of the end-of-season thickening in flooded areas took place immediately after flooding; for the December flood areas, 13 cm out of 14 cm of season-total thickening; for the January flood areas, 17 cm out of 21 cm, and for the double flooded areas, either December and February, or January and February, 26 out of 30 and 32 cm respectively. Comparing best-fit models to all thickness measurements shows that, post-flooding, the growth rate was comparable, or only slightly greater, in the test areas compared to the control areas (Figure 4a).

Mean (median) snow depth over unflooded areas (Figures 4b and Table 2) evolved from 5 (4) cm during 1–11 December, 12 (10) cm during 16–26 January, 16 (14) cm during 16–26 February, to 26 (25) cm during 3–15 May. For the test areas only flooded in December, values area 3 (4) cm during 1–11 December, 10 (10) cm during 16–26 January, 11 (12) cm during 16–26 February, to 25 (23) cm during 3–15 May. For the test areas only flooded in January, values are 2 (0) cm thick during 16–26 January, 9 (8) cm during 16–26 February, to 19 (18) cm during 3–15 May. For the test areas flooded twice, in December and February, mean snow depth evolved from 1 (1) cm thick during 16–26 February, to 17 (17) cm during 3–15 May. For the test areas flooded twice, in January and February, mean snow depth evolved from 1 (1) cm thick during 16–26 February, to 14 (13) cm during 3–15 May. Thus, despite their large variability in time and space due to wind redistribution, snow depths generally increased throughout the season, and tended to be smaller over areas that had been flooded, especially if flooded twice and/or later in the season. By the end of the growth season, all test areas had thinner snow depth relative to the control (Figure 5b), though the difference over the December-only test areas was not statistically significant.

The SIMBA profiles show that, immediately after flooding, ice temperatures warmed up from the top-down, reflecting the input of latent and sensible energy from the sea water to the sea ice. These warm pulses tended to last 2–5 days (Figure 6).

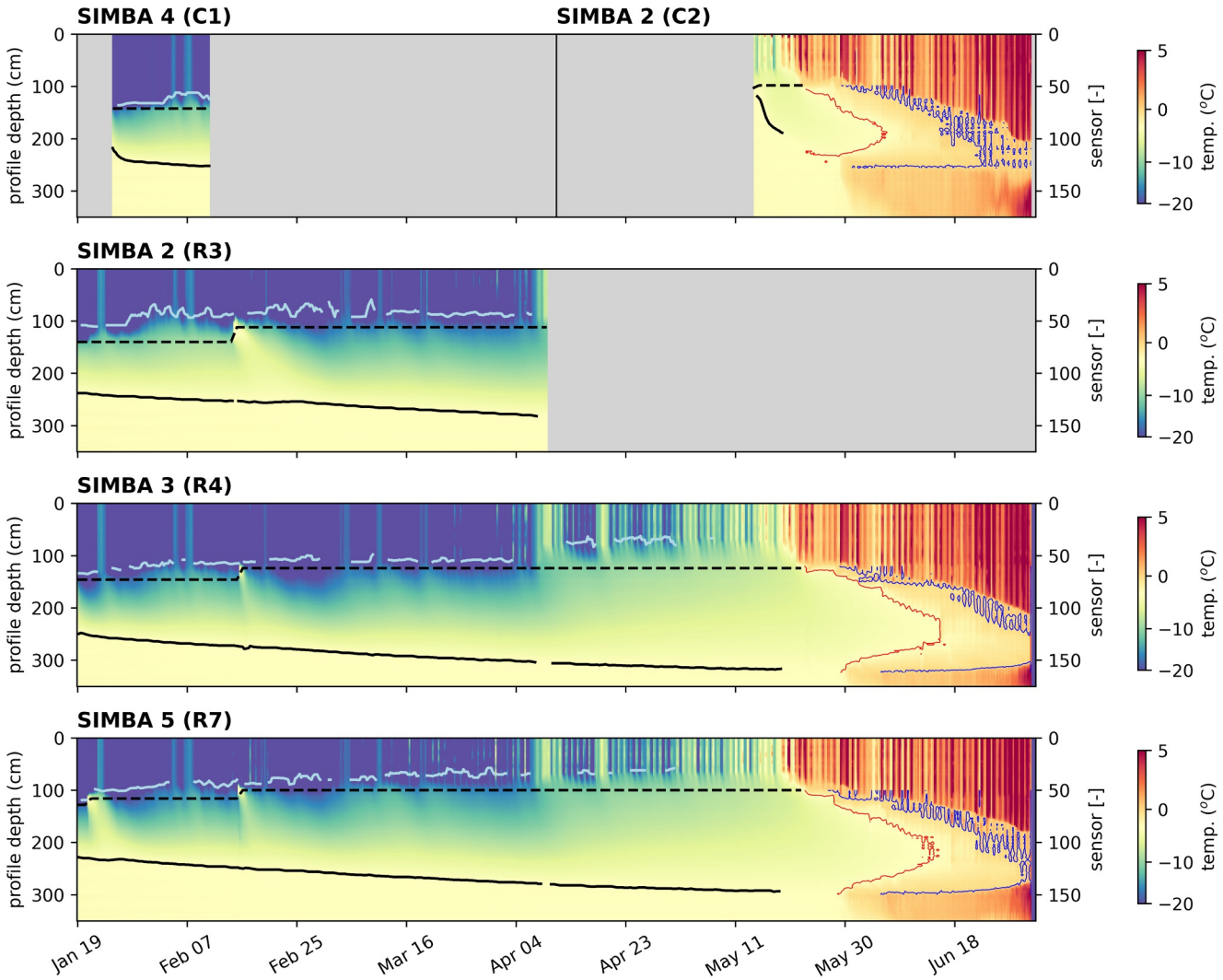


Figure 6. SIMBA 6-hourly temperature retrievals for the control C1 and C2 areas (top row), and test areas R3, R4, and R7 (second to fourth row). The dashed black line represents the estimated snow-ice interface, the bold black line represents the estimated ice-ocean interface, the light blue line represents the estimated air-snow interface. We also show the −1.51°C isotherm (the salinity-dependent freezing point, as calculated from the salinity measurements from the Cambridge Bay Underwater Network, red line) and the 0°C isotherm (blue line).

In Figure 7 we show the ice core salinity profiles. In the control areas, ice cores had C-shaped salinity profiles of relatively low values overall and small changes throughout the season. Top-and-bottom values were in the 5–7 ppt range, with lower values (1–4 ppt) in the middle of the cores. In the test areas, salinity was markedly higher in the top 20–30 cm of the profiles in the days and weeks following flooding, with values around 10–20 ppt, while below the top 30 cm, salinity values tended to be low and comparable to the control area salinity, with values in the 2–8 ppt range. The evolution of the salinity profiles throughout the winter differed across test areas. In the single-flooded December test areas, salinity profiles tended to restore toward the control profile values within 2 months of flooding. These profiles then remained low in salinity to the end of the season (with the exception of a single May profile which exhibited slightly higher values near the top of the profile). In the single-flooded January test areas, salinity at the top of the cores remained relatively high (8–12 ppt) throughout the season. In the double-flooded December and February test areas, salinity increased in the top of the profiles after flooding in December. Consistent with the single-flooded December test areas, salinity values in these test areas decreased and restored to control values prior to the second flooding (as shown by profile marked with a magenta asterisk in Figure 7). After the second-flooding in December, salinity values again increased in the top 20–30 cm of the profiles, and

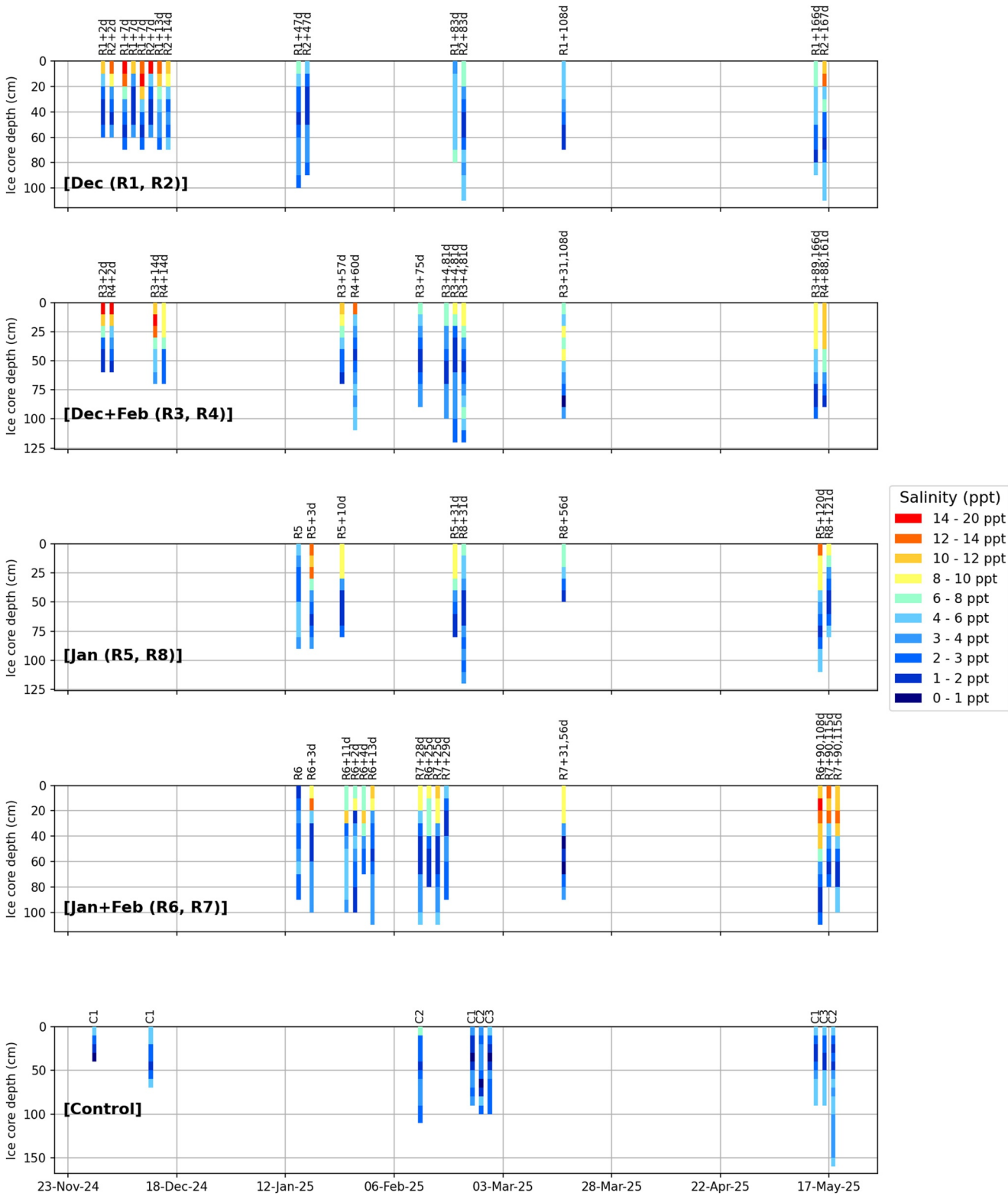


Figure 7. Salinity profiles (in ppt) of ice cores.

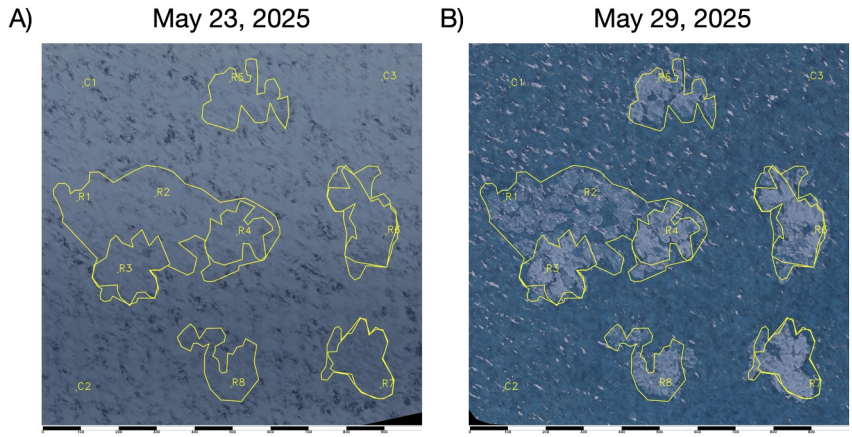


Figure 8. (a) Drone-image mosaic for the campaign site on 23 May 2025, with the outlines of the control and experiment areas shown in red, and (b) as in panel (a), but on 29 May 2025. Scale in m is shown at the bottom of the panels. The image mosaics capture the 1 × 1 km fieldsite.

remained high throughout the season. In the double-flooded January–February test areas, salinity values increased in the top 20–30 cm, and remained high throughout the whole season.

3.2. Melt Season Evolution

Surface melting was first detected on 22 May, when the air temperature rapidly climbed above 0°C (Figure 3d). Surface melt ponds started to develop by May 23, and were widespread by May 29 (Figure 8), with most of the snow cover having melted by May 29. By May 29, the test areas were significantly brighter compared to the control areas. Drone footage taken on May 28 shows that the test areas were also flooded (see Figure 9), and that the enhanced brightness was at least partly due to the sea ice itself being brighter in the test areas compared to the control areas, plausibly combined with a smaller melt pond fraction over the test areas, as estimated qualitatively from visual inspection. In situ inspection did not detect any horizontal draining from the test areas outward, implying that the reduced melt pond fraction over the test areas may in part be due to more efficient vertical drainage of meltwater through the sea ice, and/or reduced snow cover over the test areas at the start of the melt season. The enhanced brightness of the test areas was persistent throughout the melt season, as shown by ESA Sentinel imagery from May 29, June 13, June 30 and July 3 (Figure 10) and by drone imagery (Figure S4 in Supporting Information S1).



Figure 9. Image stills from a 28 May 2025 drone flight, looking northwest over test areas R7 (i.e., bottom right in Figure 8). For scale, the windsock is approximately 60 cm in length, and the wind sock post is 150 cm tall. Drone video is available in the Supporting Information S1.

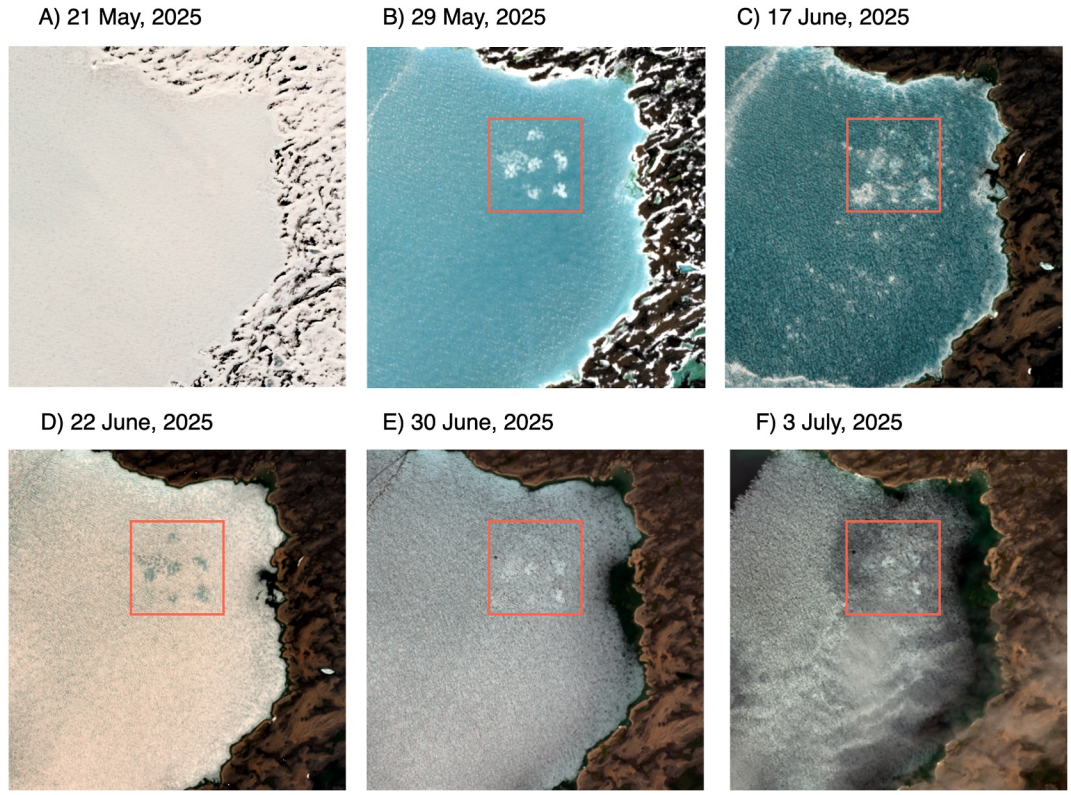


Figure 10. ESA Sentinel imagery from (a) 21 May, (b) 29 May, (c) 17 June, (d) 22 June, (e) 30 June, and (f) 3 July 2025. We show the 1 × 1 km fieldsite outlined in the red box.

On May 29, twelve 5 cm boreholes were drilled in control area C2, within an approximate 50 m radius from the center of C2. At the time, the area was mostly covered in melt ponds (Figure 11a and Figure S5 in Supporting Information S1). Daily drone and in situ monitoring over the following week observed effective draining via the boreholes, which slowly expanded to ∼0.5 m radius due to lateral melting from the water flow. By June 5, most of the C2 area had drained and was covered by bare sea ice of higher brightness (Figure 11b). This brightening over C2 was also visible from the Sentinel image on June 13 (Figure 10b).

Figure 11c shows daily values of relative luminance over 23 May–July 3 for the test areas and melt-pond drained control area C2, baselined on values taken over the unperturbed field site (control areas C1 and C3, and remaining areas outside test and control areas, referred to as supercontrol). Over the first 3 weeks of the melt season (May 23–June 17), relative luminance was greater over the test areas relative to the control areas, with areas that had been flooded twice about 30%–40% brighter, and areas that had been flooded once about 20% brighter. Luminance of the melt-pond drained control C2 area was similar to the other control areas prior to draining on May 29, and slowly increased thereafter to June 9, when C2 was 15%–20% brighter than C1 and C3. After June 17, the overall pattern reversed, and luminance over the control areas became greater for about a week (June 18–June 25). This reversal in relative brightness was due to the natural draining of melt ponds over the control areas during this time. Toward the end of June, the test areas once again exhibited greater luminance than the baseline control areas, but at more modest levels (5%–20%) than during the earlier part of the melt season.

In Figure 12a we show daily thickness values for all three SIMBAs using a bottom (ice/ocean interface) freezing point threshold of −0.5°C. For this threshold, melt rates over May 28–June 15 are slightly lower in the test areas (−3.05 cm/day and −3.29 cm/day) compared to the control area (−4.79 cm/day). This result is robust to the choice of bottom freezing point temperature (Figure 12b), with estimated melt rates in the test areas being 20%–40% lower than in the control area during late May–mid June, assuming identical bottom freezing point thresholds. These differences are to first order comparable to the differences in luminance during this period

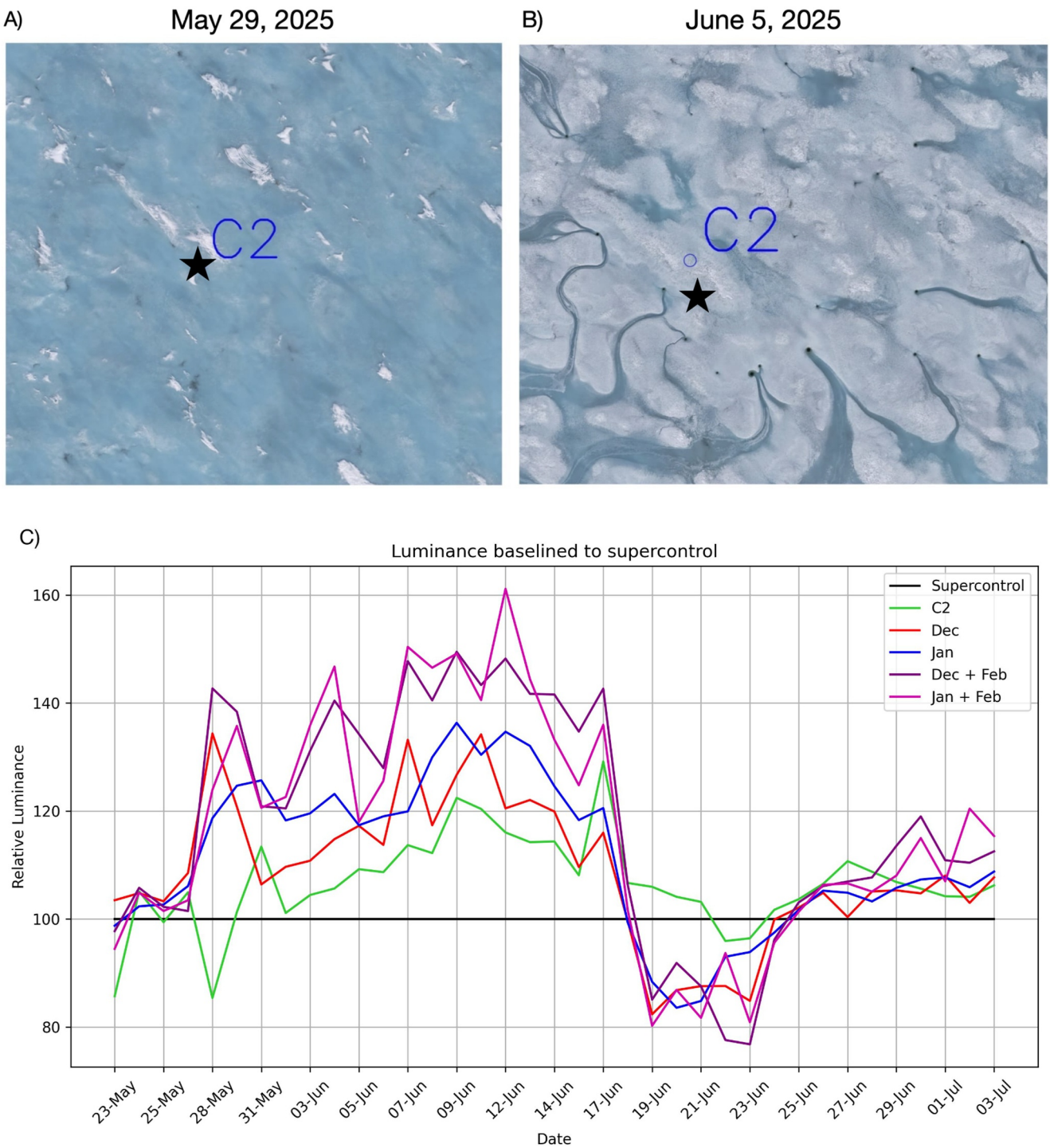


Figure 11. Drone images of C2, on (a) 29 May 2025, and (b) 5 June 2025. The images are approximately 100 m across. The black as identifies the same location in both images. (c) daily drone-estimated relative luminance averaged over the different test and control areas, baselined on control areas that were not drained (C1 and C3) and all other field site areas (referred to as supercontrol).

(Figure 11). We note that melt rates likely accelerated in the test areas around June 20 (Figure 12a), which is consistent with the timing of test areas dimming.

By late June, significant melt along the coastlines led to the sea ice becoming unfastened, followed by break up of the floe. On July 6, the three remaining SIMBA instruments were collected. In situ observations on this

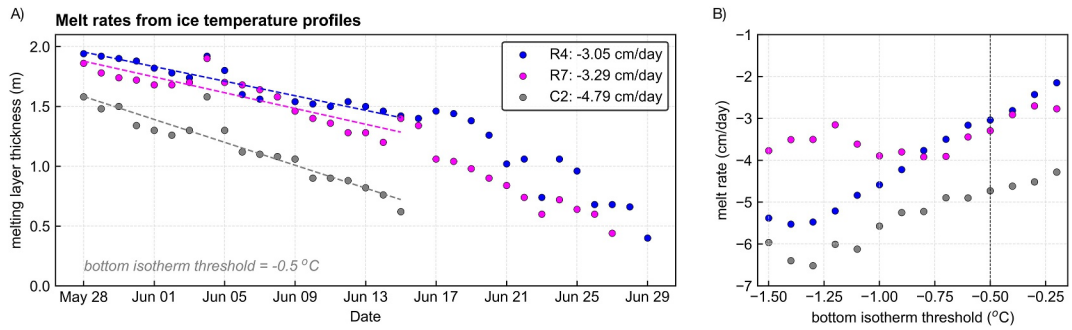


Figure 12. (a) Daily ice layer thickness as estimated by the SIMBAs for the control area C2 (gray) and test areas R4 (blue) and R7 (magenta), using a bottom freezing point threshold of 0.5°C. Average estimated melt rates over May 28–June 15 are shown in the top right legend. (b) Average melt rates for the three SIMBAs, as a function of different bottom freezing point thresholds.

date showed that the two SIMBA instruments in test areas R7 and R4 were in areas that still had ice over 40 cm thick, while the control area was mostly melted out.

4. Discussion and Conclusions

Artificially flooding Arctic sea ice during the winter to thicken it and slow down its long term decline has been recently explored in a modeling framework as a potential climate solution (Desch et al., 2017; Pauling & Bitz, 2021; Zampieri & Goessling, 2019). For the first time, we show results of a field test of sea ice flooding at a small scale in the Canadian Arctic over the sea ice growth and melt season of 2024/2025. To conduct the field test, several test areas were flooded with pumped seawater during three different time windows in December 2024 January 2025, and February 2025. We compared the effectiveness of single-flooding treatments (either in December or January) to double-flooding treatments (in December and February; or in January and February). In addition, motivated by the impact of surface melt ponds on surface albedo and sea ice melt (e.g., Perovich et al., 2007; Schröder et al., 2014), we also tested the effectiveness of melt pond draining via drilling in late May 2025 during the early part of the melt season.

We found that by the end of the ice-growth season (mid May in Cambridge Bay), sea ice in the flooded areas was thicker than sea ice in the control areas, where mean (median) sea ice thickness was 160 (161) cm. Test areas that had been flooded twice were 30–32 cm thicker, while those that had been flooded once were between 14 cm (if flooded earlier on in December) and 21 cm (if flooded later in January) thicker. In addition, we found that flooded areas tended to have a thinner snow cover, though as with sea ice thickness, these impacts were greater in the test areas flooded twice and/or later in the season.

Most of the sea ice thickening relative to the control areas (80%–90%) occurred during or immediately following the flooding treatments, after which the growth rate of the flooded areas was comparable or only slightly larger than the growth rate of the control areas. We hypothesize that the reason for the comparable rates of ice growth result from the competing effects of a reduced snow cover over the flooded areas—which itself would promote faster sea ice growth, as a thinner, less insulating snow cover promotes sea ice growth (e.g., Untersteiner, 1961), and the effect of greater ice thickness on ice growth—with thicker ice exhibiting slower rates of sea ice growth (e.g., Thorndike et al., 1975). The different observed behavior compared to that seen in modeling experiments, in which greater spring sea ice thickness results from enhanced ice growth rates (Pauling & Bitz, 2021), is likely due to modeling studies simulating an implementation that is different than the applied implementation. In Pauling and Bitz (2021), modeled flooding is applied at a much lower rate (order of magnitude lower), but constantly over a much longer period (2 months). This modeling approach never allows the model to reform a snow layer during that time, thus enhancing congelation growth relative to the real world experiment, where snow cover did build up soon after flooding.

Decadal rates of end-of-winter ice thickness in Cambridge Bay over 1980–2024 are −6 cm/decade (Howell et al., 2016), a period that has seen winter temperatures warm by almost 0.6°C per decade. Thus, 0.3 m of sea ice is

comparable to about 50 years of spring sea ice thinning in Cambridge Bay. We note that the winter of 2024/2025 was remarkably warm in Cambridge Bay, even by modern (2000 to present) standards, and may be more representative of typical conditions in coming decades, thus serendipitously providing an opportunity of testing ice thickening in "future-like" conditions at Cambridge Bay.

Flooding treatments resulted in salinity increasing in the top 20–30 cm of the ice cores. In the control areas, salinity values were generally low, and followed a C-shaped profile, with slightly higher (5–7 ppt) values in the top and bottom of the ice cores, and low (1–4 ppt) values in the middle section of the profiles. In the single-flooded December-only test areas, salinity values decreased throughout the season, and were similar to salinity profiles from the control areas within 2 months of flooding. In contrast, in the single-flooded January test areas, salinity remained slightly higher throughout the season. This may reflect the greater porosity (due to warmer temperatures) of the sea ice earlier in the season, with excess salt able to drain out easier after December flooding compared to January flooding. Salinity profiles in areas that were flooded twice remained higher than control profiles through May, with values greater than 10 ppt in the top 40–50 cm of the ice cores.

We also detected that once the melt season had started, test areas were significantly brighter than the control areas, which showed brightness consistent with sea ice in the surrounding area of the bay. We quantified luminosity daily, as monitored from a drone-mounted RGB camera. While we do not provide albedo estimates, luminance estimates, visual inspection and satellite imagery provide strong evidence that the sea ice in the flooded areas was characterized by different optical properties that led to enhanced brightness (and presumably albedo). In future work, we plan to focus on the impacts of flooding on sea ice albedo and morphology in order to further quantify and understand this response, and to better characterize changes during the melt season. We note that prior modeling efforts that have simulated sea ice flooding and its impacts (Desch et al., 2017; Pauling & Bitz, 2021; Zampieri & Goessling, 2019) do not simulate a change in sea ice albedo to flooding, which could be of importance given the influence of surface albedo on the melt rate of sea ice.

While we were unable to directly observe melt rates for the control and test areas, we have used the historical weekly Cambridge Bay fast-ice thickness data set to calculate mean weekly rates of sea ice thinning during the melt season (defined as the weeks with negative ice thickness tendency during June and July in the historical ice thickness data set). Over 1960–2023, the mean weekly rate of thinning is −3 cm/day. Melt rates estimated by the SIMBA profilers are in the −3 to −5 cm/day range. Thus, one may expect sea ice, that is, 0.3 m thicker at the beginning of the melt season to survive about 7–10 days longer. Using the SIMBA temperature profiles to estimate melt rates, we also find that the test areas likely melted at a slower rate compared to the control areas during late May–mid June, consistent with their higher brightness, and with the in situ observation at the end of the melt season in early July, when the test areas were estimated to be at least 40 cm thick as the control area melted out, suggesting additional thickening of test areas relative to the control areas during the melt season.

We have shown that artificial flooding in winter of Arctic sea ice leads to thicker and brighter sea ice by the following melt season, as well as slowing down melt, highlighting its potential use as a mitigation or local adaptation tool to help counteract future sea ice loss. We also recognize that ecological and social impacts of ice thickening need to be better understood. For example, extending the seasonal duration and extent of thicker ice would maintain vital habitat for a unique ecosystem including micro-organisms, plankton, fish, seabirds, polar bears, walruses, at least six species of seals, and Arctic communities (Divoky et al., 2024; Fay, 1982; Lund-Hansen et al., 2024; Molnár et al., 2020). At the same time, flooding sea ice in winter diminished snow depth which could impact the natal snow dens of ringed seals and polar bears (Ferguson et al., 2005; Kelly et al., 2010; Liston et al., 2016), yet longer ice seasons would also promote greater snow depths (Blanchard-Wrigglesworth et al., 2015; Hezel et al., 2012). Thickening of sea ice at scale would additionally need to consider social, economic and cultural concerns, and close collaboration with Arctic communities will be essential to inform research and applications.

Conflict of Interest

The authors declare no conflicts of interest relevant to this study.

Availability Statement

ERA5 data (Hersbach et al., 2020) are available at https://www.ecmwf.int/en/forecasts/dataset/ecmwf-reanalysis-v5, Cambridge Bay airport temperature station data are available at https://climate.weather.gc.ca/historical_data/search_historic_data_stations_e.html?searchType=stnName&timeframe=1&txtStationName=cambridge+bay&searchMethod=contains&optLimit=yearRange&StartYear=1840&EndYear=2025&Year=2025&Month=7&Day=21&selRowPerPage=25. Ice thickness measurements from Cambridge Bay from 1960 to present are available at https://www.canada.ca/en/environment-climate-change/services/ice-forecasts-observations/latest-conditions/archive-overview/thickness-data.html. Auxiliary ocean salinity data from Cambridge Bay are available from Ocean Networks Canada at https://data.oceannetworks.ca/DataSearch. ESA Sentinel-2 L2A data are available at https://eos.com/landviewer. All campaign data are available on Zenodo at (Ice, 2026).

Acknowledgments
We thank CHARS and EHTO for logisitical support in Cambridge Bay. Through MMW's postdoctoral fellowship, this material is based upon work supported by the NSF National Center for Atmospheric Research, which is a major facility sponsored by the U.S. National Science Foundation under Cooperative Agreement No. 1852977. KO is supported by the Cambridge Climate, Life and Earth (C-CLEAR) Doctoral Training Partnership funded by the U.K. Natural Environment Research Council (NE/S007164/1). This work uses ERA5 data, which contains modified Copernicus Climate Change Service information 2020. Neither the European Commission nor ECMWF is responsible for any use that may be made of the Copernicus information or data it contains.

References

Archer, L. C., Atkinson, S. N., Lunn, N. J., Penk, S. R., & Molnár, P. K. (2025). Energetic constraints drive the decline of a sentinel polar bear population. *Science*, *387*(6733), 516–521. https://doi.org/10.1126/science.adp3752

Babakhani, P., & Zarei, P. (2015). Automatic gamma correction based on average of brightness. *Advances in Computer Science: an International Journal*, *4*(6), 156–159.

Blanchard-Wrigglesworth, E., Farrell, S., Newman, T., & Bitz, C. (2015). Snow cover on Arctic sea ice in observations and an Earth system model. *Geophysical Research Letters*, *42*(23), 10–342. https://doi.org/10.1002/2015gl066049

Cavalieri, D. J., & Parkinson, C. L. (2012). Arctic sea ice variability and trends, 1979–2010. *The Cryosphere*, *6*(4), 881–889. https://doi.org/10.5194/tc-6-881-2012

Cvijanovic, I., Caldeira, K., & MacMartin, D. G. (2015). Impacts of ocean albedo alteration on Arctic sea ice restoration and northern hemisphere climate. *Environmental Research Letters*, *10*(4), 044020. https://doi.org/10.1088/1748-9326/10/4/044020

Dammann, D. O., Eicken, H., Mahoney, A. R., Meyer, F. J., & Betcher, S. (2018). Assessing sea ice trafficability in a changing Arctic. *Arctic*, *71*(1), 59–75. https://doi.org/10.14430/arctic4701

Desch, S. J., Smith, N., Groppi, C., Vargas, P., Jackson, R., Kalyaan, A., et al. (2017). Arctic ice management. *Earth's Future*, *5*(1), 107–127. https://doi.org/10.1002/2016ef000410

Divoky, G. J., Jan, P.-L., & Barbraud, C. (2024). An ice-obligate seabird responds to a multi-decadal decline in Arctic sea ice. *Ecosphere*, *15*(8), e4970. https://doi.org/10.1002/ecs2.4970

Eicken, H., & Mahoney, A. R. (2015). Sea ice: Hazards, risks, and implications for disasters. In *Coastal and marine hazards, risks, and disasters* (pp. 381–401). Elsevier.

Fay, F. H. (1982). Ecology and biology of the Pacific walrus, odobenus rosmarus divergens illiger. *North American Fauna*, *74*(74), 1–279. https://doi.org/10.3996/nafa.74.0001

Ferguson, S. H., Stirling, I., & McLoughlin, P. (2005). Climate change and ringed seal (Phoca hispida) recruitment in western Hudson Bay. *Marine Mammal Science*, *21*(1), 121–135. https://doi.org/10.1111/j.1748-7692.2005.tb01212.x

Field, L., Ivanova, D., Bhattacharyya, S., Mlaker, V., Sholtz, A., Decca, R., et al. (2018). Increasing Arctic sea ice albedo using localized reversible geoengineering. *Earth's Future*, *6*(6), 882–901. https://doi.org/10.1029/2018ef000820

Gilbert, A. L., Kay, J. E., Blanchard-Wrigglesworth, E., Bailey, D. A., Holland, M. M., Jahn, A., & Schneider, D. P. (2025). Observed winds alone cannot explain recent Arctic warming and sea ice loss. *Environmental Research: Climate*, *4*(4), 045009. https://doi.org/10.1088/2752-5295/ae11cb

Hammer, T. C., Shestov, A., van Dijke, L. L., Ypma, F., Meijeraan, T., & Hendrikse, H. (2024). Field data on sea ice restoration by artificial flooding. *Data in Brief*, *57*, 111117. https://doi.org/10.1016/j.dib.2024.111117

Hauser, D. D., Whiting, A. V., Mahoney, A. R., Goodwin, J., Harris, C., Schaeffer, R. J., et al. (2021). Co-production of knowledge reveals loss of indigenous hunting opportunities in the face of accelerating Arctic climate change. *Environmental Research Letters*, *16*(9), 095003. https://doi.org/10.1088/1748-9326/ac1a36

Hersbach, H., Bell, B., Berrisford, P., Hirahara, S., Horányi, A., Muñoz-Sabater, J., et al. (2020). The ERA5 global reanalysis. *Quarterly Journal of the Royal Meteorological Society*, *146*(730), 1999–2049. https://doi.org/10.1002/qj.3803

Hezel, P., Zhang, X., Bitz, C., Kelly, B., & Massonnet, F. (2012). Projected decline in spring snow depth on Arctic sea ice caused by progressively later autumn open ocean freeze-up this century. *Geophysical Research Letters*, *39*(17). https://doi.org/10.1029/2012gl052794

Holt, B., & Digby, S. A. (1985). Processes and imagery of first-year fast sea ice during the melt season. *Journal of Geophysical Research*, *90*(C3), 5045–5062. https://doi.org/10.1029/jc090ic03p05045

Howell, S. E., Laliberté, F., Kwok, R., Derksen, C., & King, J. (2016). Landfast ice thickness in the Canadian Arctic Archipelago from observations and models. *The Cryosphere*, *10*(4), 1463–1475. https://doi.org/10.5194/tc-10-1463-2016

Ice, R. (2026). Data collected during the winter and spring 2024/25 by Real Ice in Cambridge Bay, Canada [Dataset]. *Zenodo*. https://doi.org/10.5281/zenodo.19120738

Jackson, K., Wilkinson, J., Maksym, T., Meldrum, D., Beckers, J., Haas, C., & Mackenzie, D. (2013). A novel and low-cost sea ice mass balance buoy. *Journal of Atmospheric and Oceanic Technology*, *30*(11), 2676–2688. https://doi.org/10.1175/jtech-d-13-00058.1

Jahn, A., Holland, M. M., & Kay, J. E. (2024). Projections of an ice-free Arctic ocean. *Nature Reviews Earth & Environment*, *5*(3), 164–176. https://doi.org/10.1038/s43017-023-00515-9

Kay, J., Holland, M. M., & Jahn, A. (2011). Inter-annual to multi-decadal Arctic sea ice extent trends in a warming world. *Geophysical Research Letters*, *38*(15). https://doi.org/10.1029/2011gl048008

Kelly, B. P. (2001). Climate change and ice breeding pinnipeds. In *"fingerprints" of climate change: Adapted behaviour and shifting species ranges* (pp. 43–55). Springer.

Kelly, B. P., Bengtson, J. L., Boveng, P. L., Cameron, M. F., Dahle, S. P., Jansen, J. K., et al. (2010). Status review of the ringed seal. (phoca hispida).

Kwok, R. (2018). Arctic sea ice thickness, volume, and multiyear ice coverage: Losses and coupled variability (1958–2018). *Environmental Research Letters*, *13*(10), 105005. https://doi.org/10.1088/1748-9326/aae3ec

Laidler, G. J., Ford, J. D., Gough, W. A., Ikummaq, T., Gagnon, A. S., Kowal, S., et al. (2009). Travelling and hunting in a changing Arctic: Assessing Inuit vulnerability to sea ice change in Igloolik, Nunavut. *Climatic Change*, *94*(3), 363–397. https://doi.org/10.1007/s10584-008-9512-z

Laidre, K. L., Stirling, I., Lowry, L. F., Wiig, Ø., Heide-Jørgensen, M. P., & Ferguson, S. H. (2008). Quantifying the sensitivity of Arctic marine mammals to climate-induced habitat change. *Ecological Applications*, *18*(sp2), S97–S125. https://doi.org/10.1890/06-0546.1

Lebrun, M., Vancoppenolle, M., Madec, G., & Massonnet, F. (2019). Arctic sea-ice-free season projected to extend into autumn. *The Cryosphere*, *13*(1), 79–96. https://doi.org/10.5194/tc-13-79-2019

Lee, W. R., MacMartin, D. G., Visioni, D., Kravitz, B., Chen, Y., Moore, J. C., et al. (2023). High-latitude stratospheric aerosol injection to preserve the Arctic. *Earth's Future*, *11*(1), e2022EF003052. https://doi.org/10.1029/2022ef003052

Liston, G. E., Perham, C. J., Shideler, R. T., & Cheuvront, A. N. (2016). Modeling snowdrift habitat for polar bear dens. *Ecological Modelling*, *320*, 114–134. https://doi.org/10.1016/j.ecolmodel.2015.09.010

Lund-Hansen, L. C., Gradinger, R., Hassett, B., Jayasinghe, S., Kennedy, F., Martin, A., et al. (2024). Sea ice as habitat for microalgae, bacteria, virus, fungi, meio-and macrofauna: A review of an extreme environment. *Polar Biology*, *47*(12), 1275–1306. https://doi.org/10.1007/s00300-024-03296-z

Mahlstein, I., & Knutti, R. (2012). Arctic sea ice predicted to disappear near 2°C global warming above present. *Journal of Geophysical Research*, *117*(D6). https://doi.org/10.1029/2011JD016709

Malmgren, F., & i Bergen Geofysisk institutt, U. (1927). *On the properties of sea-ice*. AS John Griegs Boktrykkeri.

Mengis, N., Martin, T., Keller, D. P., & Oschlies, A. (2016). Assessing climate impacts and risks of ocean albedo modification in the Arctic. *Journal of Geophysical Research: Oceans*, *121*(5), 3044–3057. https://doi.org/10.1002/2015jc011433

Molnár, P. K., Bitz, C. M., Holland, M. M., Kay, J. E., Penk, S. R., & Amstrup, S. C. (2020). Fasting season length sets temporal limits for global polar bear persistence. *Nature Climate Change*, *10*(8), 732–738. https://doi.org/10.1038/s41558-020-0818-9

Nguyen, R. M., & Brown, M. S. (2017). Why you should forget luminance conversion and do something better. In *Proceedings of the ieee conference on computer vision and pattern recognition* (pp. 6750–6758).

Notz, D., & Stroeve, J. (2016). Observed Arctic sea-ice loss directly follows anthropogenic CO_2 emission. *Science*, *354*(6313), 747–750. https://doi.org/10.1126/science.aag2345

Overeem, I., Anderson, R. S., Wobus, C. W., Clow, G. D., Urban, F. E., & Matell, N. (2011). Sea ice loss enhances wave action at the Arctic coast. *Geophysical Research Letters*, *38*(17). https://doi.org/10.1029/2011gl048681

Pauling, A. G., & Bitz, C. M. (2021). Arctic sea ice response to flooding of the snow layer in future warming scenarios. *Earth's Future*, *9*(10), e2021EF002136. https://doi.org/10.1029/2021ef002136

Perovich, D. K., Light, B., Eicken, H., Jones, K. F., Runciman, K., & Nghiem, S. V. (2007). Increasing solar heating of the Arctic Ocean and adjacent seas, 1979–2005: Attribution and role in the ice-albedo feedback. *Geophysical Research Letters*, *34*(19). https://doi.org/10.1029/2007gl031480

Plante, M., Lemieux, J.-F., Tremblay, L. B., Tivy, A., Angnatok, J., Roy, F., et al. (2024). Using icepack to reproduce ice mass balance buoy observations in landfast ice: Improvements from the mushy-layer thermodynamics. *The Cryosphere*, *18*(4), 1685–1708. https://doi.org/10.5194/tc-18-1685-2024

Regehr, E. V., Lunn, N. J., Amstrup, S. C., & Stirling, I. (2007). Effects of earlier sea ice breakup on survival and population size of polar bears in western Hudson Bay. *Journal of Wildlife Management*, *71*(8), 2673–2683. https://doi.org/10.2193/2006-180

Roach, L., & Blanchard-Wrigglesworth, E. (2022). Observed winds crucial for September Arctic sea ice loss. *Geophysical Research Letters*, *49*(6), e2022GL097884. https://doi.org/10.1029/2022gl097884

Rodrigues, J. (2009). The increase in the length of the ice-free season in the Arctic. *Cold Regions Science and Technology*, *59*(1), 78–101. https://doi.org/10.1016/j.coldregions.2009.05.006

Schröder, D., Feltham, D. L., Flocco, D., & Tsamados, M. (2014). September Arctic sea-ice minimum predicted by spring melt-pond fraction. *Nature Climate Change*, *4*(5), 353–357. https://doi.org/10.1038/nclimate2203

Stuecker, M. F., Bitz, C. M., Armour, K. C., Proistosescu, C., Kang, S. M., Xie, S.-P., et al. (2018). Polar amplification dominated by local forcing and feedbacks. *Nature Climate Change*, *8*(12), 1076–1081. https://doi.org/10.1038/s41558-018-0339-y

Thorndike, A. S., Rothrock, D. A., Maykut, G. A., & Colony, R. (1975). The thickness distribution of sea ice. *Journal of Geophysical Research*, *80*(33), 4501–4513. https://doi.org/10.1029/jc080i033p04501

Tilmes, S., Jahn, A., Kay, J. E., Holland, M., & Lamarque, J.-F. (2014). Can regional climate engineering save the summer Arctic sea ice? *Geophysical Research Letters*, *41*(3), 880–885. https://doi.org/10.1002/2013gl058731

Untersteiner, N. (1961). On the mass and heat budget of Arctic sea ice. Archiv für Meteorologie, Geophysik und Bioklimatologie. *Serie A*, *12*(2), 151–182. https://doi.org/10.1007/bf02247491

Webster, M. A., & Warren, S. G. (2022). Regional geoengineering using tiny glass bubbles would accelerate the loss of Arctic sea ice. *Earth's Future*, *10*(10), e2022EF002815. https://doi.org/10.1029/2022ef002815

Zampieri, L., & Goessling, H. F. (2019). Sea ice targeted geoengineering can delay Arctic sea ice decline but not global warming. *Earth's Future*, *7*(12), 1296–1306. https://doi.org/10.1029/2019ef001230